Optical properties of ZnTe/ZnSe core/shell nanowire

S. I. GEORGESCU[*], S. MICLUŢA-CÂMPEANU
Faculty of Physics, University of Bucharest, Bucharest 077125, Romania

Within the effective mass approximation the sub-band energy structure of semiconductor cylindrical core/shell nanowires is simulated. The heteroepitaxial strain of the core-shell heterostructure is modeled by the elastic continuum approach within an isotropic treatment. The general equilibrium equation, Hooke's law and interface boundary matching condition are used in the strain modeling. The analytical results are applied to ZnTe/ZnSe, a wide band gap type-II heterostructure. Localization of the photoexcited electron-hole carriers and oscillator strength are investigated as function of the shell thickness. The calculated oscillator strengths are in accordance with previous reported results.

1. Introduction

One-dimensional quantum confined semiconductors are of large interest from both theoretical and technological perspectives in the recent past. Thus, nanowires have been investigated for improving optical absorption [1-4] and charge separation [5,6] in photovoltaic devices. Current transport in nanowire resonant tunneling diodes has been investigated in view of downscaling of integrated circuits [7,8]. The progress in crystal growth has led to the fabrication of regular and stable core/shell nanowires structures [9], which allow the optical and transport properties of such elongated nanostructures to be tuned. Confining charge carriers to the shell is important in photovoltaic devices for an efficient collection. Confinement is the result of two physical phenomena, namely, (i) band alignment and (ii) strain-engineering of the core/shell structures. At the contact of two different crystals band alignment induces a potential confinement, which is modified by the strain field induced by lattice mismatch. As a result, the band gap is modified, and consequently the electronic structure and the electrical and optical properties of the heterostructure are changed. For example, for an accurate simulation of the (multi)excitonic spectra the strain should be carefully taken into account as it influences the effective masses of the carriers [10] or frequencies of optical phonons modes [11,12]. In spintronics, in the storage and computing electronic devices, the strain is one of the control parameters. For example, in the intrinsic spin Hall effect, the conductivity of a two-dimensional electronic gas is influenced by both magnetic and strain fields [13,14].

Within the continuum elasticity, the strain field in isotropic or anisotropic crystal heterostructures is obtained by either (i) solving the elasticity equilibrium equation or (ii) by minimizing the elastic energy stored in the nanostructure[15]. The theoretical investigations of elastic properties of heterostructures experiencing pseudomorphic strain are mainly based on analytical Eshelby's work [16] on elastic inclusions. In hetero-nanostructures, this method is applied in often applied (see, e.g. Refs. [17-19]). The main requirement in Eshelby's treatment applicability is that the matrix (the embedding material) is infinite. In the present work, we investigate core/shell structures with finite size of the shell (matrix) and consequently an elasticity modeling of hetero-nanostructures that takes into account this aspect should be adopted. The structure we model is ZnTe/ZnSe shell nanowire (CSNW), a type II heterostructure (see classification of heterostructures as function of their band alignments in, e.g., Ref. [20]). The paper is structured as follows.

In section 2, we present the theory used in describing the strain field and the single particle states (SPSs) of the CSNW. In section 3, we present the results, the photo-excited carriers location and the oscillator strengths of the CSNW. Section 4 contains the conclusions.

2. Theory

First, based on Refs. [21-24], we briefly introduce the lattice mismatch strain field model for CSNW. Within this model, the strain distribution is obtained by solving the linear elasticity equilibrium equation. We consider an infinite length and isotropic CSNW (elastic constants are position independent in each of the two components, core and shell). One approximates the displacement as having radial symmetry, $\mathbf{u} = (u_r(r), 0, 0)$, and the axial strain tensor components as $e_{zz}^A(z) = \varepsilon_0$ and $e_{zz}^B(z) = 0$. This approximation, which holds in limit of long CSNW and thick shell, makes the displacement field irrotational. Then, within the continuum elasticity approach the equilibrium equation is simply: grad div $\mathbf{u} = 0$ [25]. The linear stress (σ_{ij})-strain (ε_{ij}) tensor relation is used and the following boundary conditions are imposed:

(i)   continuous   stress   at   the interfaces, $\sigma_{rr}^{A}(r_0) = \sigma_{rr}^{B}(r_0)$,

(ii) vanishing pressure outside CSNW, $\sigma_{rr}^{B}(R) = 0$,

(iii) shrink-fit induced by the lattices mismatch, $u_r^A(r_0) - u_r^B(r_0) = \varepsilon_0 r_0$,

where r_0 is the core radius, R is the core+shell radius and $\varepsilon_0 = (a_B - a_A)/a_A$ is the relative lattice mismatch (A, B, denote the core, and shell, respectively). Then, the following strain tensor components in cylindrical coordinates are obtained [24]:

$$e_{rr}^A = e_{\theta\theta}^A = \varepsilon_0 C^{AB}\left[1 - \nu_A\left(\frac{1}{C^{AB}} - 1\right)\right], \quad (1.a)$$

$$e_{hyd}^A = \varepsilon_0 C^{AB}\left(3 + \left(\frac{1}{C^{AB}} - 1\right)(1 - 2\nu_A)\right), \quad (1.b)$$

$$e_r^B(r) = -\varepsilon_0 C^B \frac{E_B}{E_A}\left(1 - \frac{R^2/r^2}{1 - 2\nu_A}\right), \quad (1.c)$$

$$e_{\theta\theta}^B(r) = -\varepsilon_0 C^B\left(\frac{R^2/r^2}{1 - 2\nu_A} + 1\right), \quad (1.d)$$

$$e_{hyd}^B = -2\varepsilon_0 C^B(1 - 2\nu_B), \quad (1.e)$$

where $C^{AB} = \left[1 + \frac{E_A}{E_B}\frac{1 + \nu_B}{1 + \nu_A}\frac{1 + (1 - 2\nu_B)r_0^2/R^2}{(1 - 2\nu_A)(1 - r_0^2/R^2)}\right]^{-1}$ and

$C^B = C^{AB}\frac{E_A}{E_B}\frac{1 + \nu_B}{R^2/r_0^2 - 1}$; E_A, E_B are Young modulus and

ν_A, ν_B Poisson ratios of the core and shell, respectively.

Second, we model the heterostructures band lineup. In semiconductor lattice-mismatch heterostructures the epitaxial strain induces deformations that shift both valence band (VB) and conduction band (CB) edges. The values of the VB and CB extrema at the Γ point (we consider direct band semiconductors) are given by [26]:

$$E_{v,c} = E_{v,c}^u + a_{v,c}e_{hyd} , \quad (2)$$

where the unstrained values are related by $E_c^u = E_v^u + E_g$ and E_g is the unstrained bandgap, $a_{v,c}$ is the volume deformation potential (subscript v for VB, c for CB), and e_{hyd} is the hydrostatic strain. For the VB, we denote the bandoffset as $V_h = E_v^A - E_v^B$ where index h holds for hole states as is schematically represented in Fig. 1.

For the CB, we denote the bandoffset as $V_e = E_c^A - E_c^B$, where index e holds for electronic states. According to this model, we have for the CSNW in cylindrical coordinates the following potentials as functions of r:
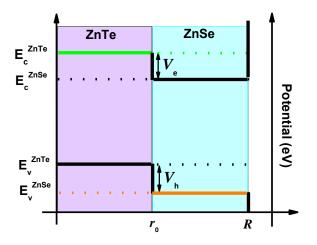

Fig. 1 Schematic band lineup in presence of strain for the type II heterostructure, ZnTe/ZnSe CSNW

1)   for electrons
$$V(r) = \begin{cases} V_e, \text{ if } 0 \le r < r_0 \\ 0, \text{ if } r_0 \le r < R \\ \infty, \text{ if } r \ge R \end{cases} ,$$

2)   for holes
$$V(r) = \begin{cases} 0, \text{ if } 0 \le r < r_0 \\ V_h, \text{ if } r_0 \le r < R \\ \infty, \text{ if } r \ge R \end{cases} .$$

In order to obtain the energy levels, we use the one-particle Schrödinger equation in the effective mass and envelope wave function approximations. In cylindrical coordinates $\mathbf{r} = (r, \theta, z)$, Schrödinger equation of the envelope wave functions reads [27]:

$$\left(\frac{1}{\mu_\perp}\frac{d^2}{dr^2} + \frac{1}{r\mu_\perp}\frac{d}{dr} + \frac{1}{\mu_\perp r^2}\frac{d^2}{d\theta^2} + \frac{1}{\mu_\parallel}\frac{d^2}{dz^2}\right)\Psi$$
$$= \frac{-2}{\hbar^2}(E - V)\Psi \quad (3)$$

where $\mu_\perp$ is the effective mass of the charge carrier in the xy plane and $\mu_\parallel$ is the effective mass along the z axis. Taking into consideration the form of the wave function, $\Psi_{mk}(\mathbf{r}) = R_m(r)e^{im\theta}e^{icz}$ and using the notation $\varepsilon = E - (\hbar^2/2\mu)k^2$, with $k = c\sqrt{\mu_\perp/\mu_\parallel}$ and $\mu = \mu_\perp$, Eq. (3) reduces to the differential equation:

$$r^2\frac{d^2 R_m}{dr^2} + r\frac{dR_m}{dr}$$
$$+ \left[\frac{2\mu}{\hbar^2}(\varepsilon - V)r^2 - m^2\right]R_m = 0 \quad (4a)$$

Using the change of variable, $\rho = k_i r$, where $k_i^2 = -2\mu_i(E - V_i)/\hbar > 0$ if $E < V_i$ and $k_i^2 = 2\mu_i(E - V_i)/\hbar > 0$ if $E > V_i$ (with the notations, $\mu_i = \mu_i^{e,h}$ for the effective mass of the electron (e) or hole (h) in the core ($i=A$) or shell ($i=B$), and V_i for the values of the piecewise-constant potential in region i, that is, $V_i = 0$ or $V_{e,h}$), and considering $R_m(r) = v_m(\rho)$, Eq. (4a) reduces to the Bessel differential equation:

$$\rho^2 \frac{d^2 v_m(\rho)}{d\rho^2} + \rho \frac{dv_m(\rho)}{d\rho}$$
$$+ \left(\mp \rho^2 - m^2\right) v_m(\rho) = 0 \qquad (4b)$$

Depending on the values of V and ε, we have the following cases: a) if $\varepsilon > V$, Eq. (4b) reduces to a Bessel differential equation having as solution a linear combination of Bessel functions of the first kind, J_m, and Bessel functions of the second kind, Y_m; ii) if $\varepsilon < V$ Eq. (4b) reduces to a modified Bessel differential equation having as solution a linear combination of modified Bessel functions of the first kind, I_m, and Bessel functions of the second kind, K_m

For electron states, to get regular solution on z axis: if $\varepsilon < V_e$ we disregard the modified Bessel function of the second kind K_m, and if $\varepsilon > V_e$ we disregard the Bessel function of the second kind Y_m. Then, for the core we have the following cases: i) if $\varepsilon < V_e$, the solution is of the form $R_m^{(1)}(r) = A_m I_m(k_1 r)$, with $k_1 = \sqrt{2(V_e - \varepsilon)\mu_A^e}/\hbar$, and ii) if $\varepsilon > V_e$ the solution is of the form $R_m^{(2)}(r) = B_m J_m(k_2 r)$, with $k_2 = \sqrt{2(\varepsilon - V_e)\mu_A^e}/\hbar$. In the shell, where $V = 0$, we have no restrictions and the solution is of the form, $R_m^{(3)}(r) = C_m J_m(kr) + D_m Y_m(kr)$. For the case $\varepsilon < V_e$, the boundary conditions are as follows:

$$\begin{cases} R_m^{(1)}(r_0) = R_m^{(3)}(r_0) \\ \left.\dfrac{1}{\mu_A} \dfrac{dR_m^{(1)}(r)}{dr}\right|_{r_0} = \left.\dfrac{1}{\mu_B} \dfrac{dR_m^{(3)}(r)}{dr}\right|_{r_0} \\ R_m^{(3)}(R) = 0 \end{cases} \qquad (5a)$$

After replacing $R_m^{(1)}, R_m^{(3)}$ in Eq. (5a), we obtain the transcendental equation:

$$\frac{\mu_B^e}{\mu_A^e} \frac{I_m'(k_1 r_0)}{I_m(k_1 r_0)}$$
$$= \frac{J_m'(k_3 r_0)Y_m(k_3 R) - J_m(k_3 R)Y_m'(k_3 r_0)}{J_m(k_3 r_0)Y_m(k_3 R) - J_m(k_3 R)Y_m(k_3 r_0)}, \qquad (5b)$$

where I_m', J_m', Y_m' are the first derivatives of the Bessel functions and modified functions with respect to r. The orthonormalization equation for this case is:

$$|A_m|^2 \int_0^{r_0} r \, |I_m(k_1 r)|^2 \, dr$$
$$+ \int_{r_0}^R r \, |C_m J_m(k_3 r) + D_m Y_m(k_3 r)|^2 dr = 1/4\pi^2 \qquad (5c)$$

The energy of the electron SPSs is obtained by solving the transcendental equation. Introducing the energy levels into the orthonormalization equation, we calculate the orthonormalization constants and obtain the form of the radial component of the wave function $R_m(r)$. Similarly, for the case $\varepsilon > V_0$, by replacing the index (1) by (2) in Eq. (5a), we obtain the transcendental equation:

$$\frac{\mu_B^e}{\mu_A^e} \frac{J_m'(k_1 r_0)}{J_m(k_1 r_0)}$$
$$= \frac{J_m'(k_3 r_0)Y_m(k_3 R) - J_m(k_3 R)Y_m'(k_3 r_0)}{J_m(k_3 r_0)Y_m(k_3 R) - J_m(k_3 R)Y_m(k_3 r_0)}, \qquad (6a)$$

where J_m', Y_m' are the first derivatives of the Bessel modified functions, with respect to r. The orthonormalization equation reads:

$$|B_m|^2 \int_0^{r_0} r \, |J_m(k_2 r)|^2 \, dr$$
$$+ \int_{r_0}^R r \, |C_m J_m(k_3 r) + D_m Y_m(k_3 r)|^2 dr = 1/4\pi^2 \qquad (6b)$$

For hole states, according to the effective mass approximation model, we take into account the heavy and light holes. We consider the spherical part of the heavy-hole masss (μ^{hh}) and light-hole masses (μ^{lh}) assumed by the parabolic dispersion of the one-band model [21],

$$\mu^{hh(lh)} = \frac{m_0}{\gamma_1}\left[1 - (+)\frac{6\gamma_3 + 4\gamma_2}{5\gamma_1}\right] \qquad (7)$$

Consequently, to obtain the energy structure we collect the two kinds of hole SPSs. In the core, the solution of the radial component is $R_m^{(1)}(r) = A_m J_m(k_1 r)$, where $k_1 = \sqrt{2\varepsilon \mu_A^h}/\hbar$. In the shell, for $\varepsilon < V_h$,

$$R_m^{(2)}(r) = B_m I_m(k_2 r) + C_m K_m(k_2 r),$$

where $k_2 = \sqrt{2(V_h - \varepsilon)\mu_B^h}/\hbar$ and for $\varepsilon > V_h$,

$$R_m^{(3)}(r) = D_m J_m(k_3 r) + E_m Y_m(k_3 r),$$

where $k_3 = \sqrt{2(\varepsilon - V_0)\mu_B^h}/\hbar$. Then, we impose similar boundary conditions as in the case of electronic states. In the first case, $\varepsilon < V_h$,

$$\begin{cases} R_m^{(1)}(r_0) = R_m^{(2)}(r_0) \\ \dfrac{1}{\mu_A^h}\dfrac{dR_m^{(1)}(r)}{dr}\bigg|_{r_0} = \dfrac{1}{\mu_B^h}\dfrac{dR_m^{(2)}(r)}{dr}\bigg|_{r_0} \\ R_m^{(2)}(R) = 0 \end{cases}, \quad (8a)$$

and we obtain the transcendental equation:

$$\frac{\mu_B^h}{\mu_A^h}\frac{J_m'(k_1 r_0)}{J_m(k_1 r_0)} = \frac{I_m'(k_2 r_0)K_m(k_2 R) - I_m(k_2 R)K_m'(k_2 r_0)}{I_m(k_2 r_0)K_m(k_2 R) - I_m(k_2 R)K_m(k_2 r_0)}, \quad (8b)$$

and the orthonormalization equation,

$$|A_m|^2 \int_0^{r_0} r\,|J_m(k_1 r)|^2\,dr + \int_{r_0}^R r\,|B_m I_m(k_2 r) + C_m K_m(k_2 r)|^2\,dr = 1/4\pi^2 . \quad (8c)$$

In the second case, $\varepsilon > V_0$, by replacing the index (2) by (3) in Eq. (8a), the transcendental equation reads:

$$\frac{\mu_B^h}{\mu_A^h}\frac{J_m'(k_1 r_0)}{J_m(k_1 r_0)} = \frac{J_m'(k_3 r_0)Y_m(k_3 R) - J_m(k_3 R)Y_m'(k_3 r_0)}{J_m(k_3 r_0)Y_m(k_3 R) - J_m(k_3 R)Y_m(k_3 r_0)}, \quad (9a)$$

and the orthonormalization equation is

$$|A_m|^2 \int_0^{r_0} r\,|J_m(k_1 r)|^2\,dr + \int_{r_0}^R r\,|D_m J_m(k_3 r) + E_m Y_m(k_3 r)|^2\,dr = 1/4\pi^2 . \quad (9b)$$

3. Application to ZnTe/ZnSe core/shell nanowires

As a result of weak mixing of the hole states in wide bandgap heterostructures [28], the orbitals obtained by the one-band model are close to the realistic ones. The band lineup of ZnTe/ZnSe CSNW in presence of strain at Γ point is obtained by using the model-solid theory of Van de Walle [26] with the material parameters from Table 1. Direction dependence of the effective masses is disregarded for the Γ point in Eq. (3). From Ref. [33], the bulk (unstrained) values are: $E_c^{uZnTe} = -3.09$, $E_c^{uZnSe} = -3.38eV$, $E_v^{uZnTe} = -5.34$, $E_v^{uZnSe} = -6.07eV$. With these bulk values of the band edge from Eqs. (1) and (2) (with $\varepsilon_0 = -0.071$) by using the fact ZnTe and ZnSe are direct band semiconductors, we find the band lineup

and the electron and hole SPSs in presence of strain at Γ point as function of R and r_0 as shown in Fig. 2.

Table 1. Material parameters used in the work.

	ZnTe	ZnSe
a (Å)	6.08[a]	5.65[a]
E (10^{10} Nm^{-2})	4.17[a]	4.51[a]
ν	0.363[a]	0.376[a]
E_{gap} (eV)	2.25[e]	2.69[e]
E_v (eV)	-5.34[e]	-6.07[e]
a_v (eV)	0.79[f]	1.65[f]
a_c (eV)	-5.83[f]	-4.17[f]
γ_1	3.74[g]	3.77[g]
γ_2	1.07[g]	1.24[g]
γ_3	1.64[g]	1.67[g]
$\mu^{lh\ i}$	0.152	0.148
$\mu^{hh\ i}$	1.092	1.292
μ^e	0.20[j]	0.21[j]

[a]Ref.[29]; [b]Ref.[30]; [c]Ref.[31]; [d]Ref.[32]; [e]Ref.[33]; [f]Ref.[26]; [g]Ref.[34]; [h]Ref.[35]; [i]calculated with Eq. (7).

We obtain that the strain induces enlargement (shrinkage) of the band gap for ZnTe (ZnSe), and the band gaps, $E_g^{ZnTe} = E_c^{ZnTe} - E_v^{ZnTe}$, $E_g^{ZnSe} = E_c^{ZnSe} - E_v^{ZnSe}$ increase with the shell thickness. As shown in Fig. 2a, the electron energy decreases with the shell thickness, which results in decreasing of the lowest energy transition, in accordance with the results regarding the absorption and emission spectra reported by Bang *et al.* [36] for ZnTe/ZnSe CS quantum dots. On the other hand, one can see the hole energies in Fig. 2b remain practically not affected by the shell thickness. The first four hole energy levels are of heavy hole type and for larger radii R the first light hole is almost superposed over a heavy hole energy.

The square of the radial part of the envelope wave function multiplied by r is shown in Fig. 3 for the first two electron and hole energy levels. One can see that for thin enough shell the electron ground state has a significant localization in the core and with the thickness increase the ground state is localized in the shell. This prediction has a practical importance in design of photovoltaic CSNWs, where separation of the electron and hole facilitates the charge carriers separation. The hole is confined in the core.
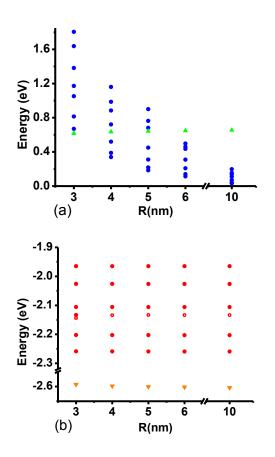
Fig. 2 Energy of the first seven electron (blue color) and hole (red color) single particle states in ZnTe/ZnSe CSNW at Γ point. Core radius is r_0=2nm. Continuum lines with up (down) triangle symbols show the band lineup in presence of lattice mismatch strain of electron (hole) states for ZnTe-green color, ZnSe-orange color. Zero reference is ZnSe CB edge, see Fig. 1. First appeared light hole state is represented as a hollow disk; it is almost superposed on a heavy hole state.

The optical spectra can be described by the oscillator strength [21,37],

$$f_{ij} = \frac{E_P}{\hbar \omega_{ij}} \left| \left\langle \psi_{mk}^* \middle| \psi_{m'k'} \right\rangle \right|^2, \tag{10}$$

which characterizes the probability of interband transition between two SPSs, i (characterized by the set of quantum numbers, m,k) and j (characterized by the set of quantum numbers, m',k'); $E_P = 2m_0 \left| P \right|^2 / \hbar^2$ and $P = -i(\hbar / m_0) \left\langle s \middle| p_x \middle| x \right\rangle$ is the Kane momentum matrix element. In Fig. 4 we present the influence of the shell thickness on the oscillator strength obtained from the first seven hole and electron SPSs shown in Fig. 2 for $E_P = 19.1$eV [34]. A larger overlap of the envelope wave functions determine a stronger oscillator strength.

The same characteristic observed for CS quantum dots, namely, thicker shell leads to a decrease of the oscillator strength [21, 23] remains valid for CSNWs. Also a continuous red shift of the lowest energy transition, **11** (as denoted in Fig. 4) with the shell thickness is obtained, similarly to the experiment [36].
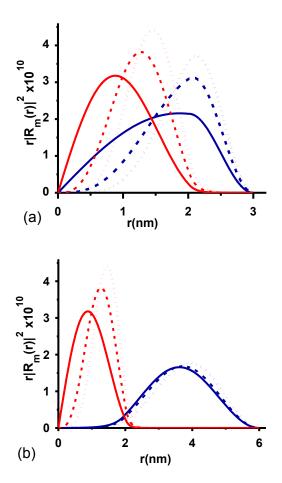

Fig. 3 Probability density of the first three SPSs for type-II ZnTe/ZnSe CSNW, $r \left| R_m(r) \right|^2$ electron (blue color) and hole (red color): (a) R=3nm; (b) R=6nm. Continuous line - first state; dashed line - second state; dotted line - third state.

In absence of experimental results, in Fig. 5, we compare the absorption results obtained by Bang et al. [36] for CS quantum dots with our simulated results, for ZnTe/ZnSe CS NWs with $r_0 = 2$nm as function of shell thickness. We assign the lowest energy transition, **11**, active one as shown in Fig. 5 to the main peak recorded in Ref. [36] in absorbance measurements. The agreement is satisfactory and it encourages comparison of our model to the experimental results for absorption in ZnTe/ZnSe CS NWs.
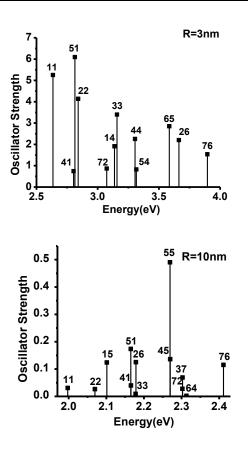
4. Conclusions

Within the one-band model effective mass approximation a strain continuum elastic model is applied to predict the energy structure of CS NWs and oscillator strengths. The model is applied to a type II direct wide band gap ZnTe/ZnSe heterostructure. The results are obtained for the Γ point by considering both heavy and light hole states. Given the good results obtained within one-band model for Znte/ZnSe quantum dots, we expect the present results to be a valid guide in description of the optical absorption in such heterostructures. The present study confirms the importance of the heteroepitaxial strain in modeling of core/shell mismatch nanostructures. We think the present approach is a very useful model for at least preliminary calculations of the optical properties of type-II CS NWs of wide band gap, where the band mixing effect is of less importance.

Fig.4 Oscillator strengths at Γ point for ZnTe/ZnSe CSNW with core radius r_0=2nm and (a) R=3nm, (b) R=10nm. In the label the first digit represents the hole states and the second electron state. The digits from 1 to 7 are associated to the number of the state in ascending order.
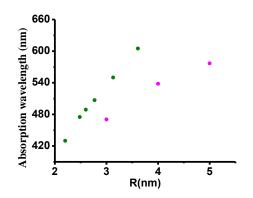

Fig. 5 Absorption wavelength for ZnTe/ZnSe: (a) CS quantum dot with r_0=2nm; (b) CSNW with r_0=2nm. The legend: ● - experimental values and ● - simulated values, as function of the total radius R. The simulation is obtained for the lowest energy transition corresponding to the transition 11 in Fig. 4.

References

[1] E. Garnett, P.Yang, Nano Lett. **10**, 1082 (2010).
[2] J. Li, H.Y. Yu, S.M. Wong, X. Li, G. Zhang, P. G.-Q. Lo, D.-L. Kwong, Appl. Phys. Lett **95**, 243113 (2009).
[3] H. Bao, X. Ruan, Opt. Letters **35**, 3378 (2010).
[4] M. M. Adachi, M. P. Anantram, K. S. Karim, Nano Lett. **10**, 4093 (2010).
[5] M. Law, L. E. Greene, J. C. Johnson, R. Saykally, P. Yang, Nature Mat. **4**, 455 (2005).
[6] B. M. Kayes, H. A. Atwater, N. S. Lewis, J. Appl. Phys. **97**, 114302 (2005).
[7] M. Björk, B. Ohlsson, C. Thelander, A. Persson, K. Deppert, L. Wallenberg, L. Samuelson, Appl Phys Lett **81**, 4458 (2002).
[8] M. Zervos, Nanoscale Research Letters **9**, 509 (2014).
[9] L. J. Lauhon, M. S. Gudiksen, D. Wang, C. M. Lieber, Nature **420**, 57 (2002).
[10] T. O. Cheche, EPL **86**, 67011 (2009).
[11] M. P. Chamberlain, M. Cardona, B. K. Ridley, Phys. Rev. **B 48,** 14356 (1993); T.O. Cheche, M.C. Chang, Chem. Phys. Lett. **406** 479 (2005).
[12] S. N. Klimin, V. M. Fomin, J. T. Devreese, D. Bimberg, Phys. Rev. **B 77**, 045307 (2008).
[13] T. O. Cheche, Phys. Rev. **B 73**, 113301 (2006).
[14] T. O. Cheche, E. Barna, Appl. Phys. Lett. **89**, 042116 (2006).
[15] C. Pryor, J. Kim, L. W. Wang, A. J. Williamson, A. Zungera, J. Appl. Phys. **83**, 5 (1998).
[16] J. D. Eshelby, Proc. R. Soc. London, Ser. A **241**, 376 (1957).

[17] V. G. Stoleru, D. Pal, E. Towe, Physica E
     15, 131 (2002).
[18] A. D. Andreev, J. R. Downes, D. A. Faux,
     E. P. O'Reilly, J. Appl. Phys. **86**, 297 (1999).
[19] T. O. Cheche, Y.-C. Chang, J. Appl. Phys.
     104, 083524 (2008).
[20] M. E. Pistol, C. E. Pryor, Phys. Rev. B
     78, 115319 (2008).
[21] T. O. Cheche, V. Barna, Y. C. Chang, Superlattice
     Microstruct. **60,** 475 (2013).
[22] T. O. Cheche, V. Barna, I. Stamatin, J Optoelectron
     Adv. Mater. **15**, 615 (2013).
[23] T. E. Pahomi, T. O. Cheche, Chem. Phys. Lett.
     612, 33 (2014).
[24] T. E. Pahomi, S. B. Stanciu, J Optoelectron Adv.
     Mater. **16**, 501 (2014).
[25] L. D. Landau, E.M. Lifshitz, Theory of Elasticity,
     Pergamon, 1970.
[26] C. G. Van de Walle, Phys. Rev. **B 39**, 1871 (1989).
[27] G. Bastard, Wave mechanics applied to
     semiconductor heterostructures, EDP Sciences
     (1992)
[28] P. C. Sercel, K. J. Vahala, Phys. Rev. B
     42, 3690 (1990).

[29] D. Belincourt, H. Jaffe, L.R. Shiozawa, Phys. Rev.
     129, 1009 (1963).
[30] Y.H. Li, X.G. Gong, S.H. Wei, Phys Rev B
     73, 245206 (2006).
[31] R.B. Hall, J.D. Meakin, Thin Solid Films
     63, (1979) 203.
[32] S. Adachi, Properties of Group-IV, III-V and II-VI
     Semiconductors, John Wiley & Sons, Chichester,
     2005.
[33] S. S. Lo, T. Mirkovic, C. H. Chuang, C. Burda,
     G. D. Scholes, Adv Mater **23,** 180 (2011).
[34] P. Lawaetz, Phys Rev B **4,** 3460 (1971).
[35] D. Mourad, J.P. Richters, L. Gerard, R. Andre,
     J. Bleuse, H. Mariette, ArXiv:1208.2188v2.
[36] J. Bang, J. Park, J.H. Lee, N. Won, J. Nam, J. Lim,
     B.Y. Chang, H.J. Lee, B. Chon, J. Shin, J.B. Park,
     J.H. Choi, K. Cho, S.M. Park, T. Joo, S. Kim, Chem.
     Mater. **22,** 233 (2010).
[37] J. H. Davies, The Physics of Low-Dimensional
     Semiconductors: An Introduction, Cambridge
     University Press, Cambridge, 1996, p.318.

_____

[*]Corresponding author: silviageorgescu451@yahoo.com